J|A|C|S
ARTICLES
Published on Web 05/20/2004

Multiple-Quantum Relaxation Dispersion NMR Spectroscopy Probing Millisecond Time-Scale Dynamics in Proteins: Theory and Application

Dmitry M. Korzhnev, Karin Kloiber, and Lewis E. Kay*

Contribution from the Protein Engineering Network Centres of Excellence and the Departments of Medical Genetics, Biochemistry and Chemistry, University of Toronto, Toronto, Ontario, Canada M5S 1A8

Received January 2, 2004; E-mail: kay@pound.med.utotonto.ca

Abstract: New relaxation dispersion experiments are presented that probe millisecond time-scale dynamical processes in proteins. The experiments measure the relaxation of $^{1}H-^{15}N$ multiple-quantum coherence as a function of the rate of application of either ^{1}H or ^{15}N refocusing pulses during a constant time relaxation interval. In contrast to the dispersion profiles generated from more conventional $^{15}N(^{1}H)$ single-quantum relaxation experiments that depend on changes in $^{15}N(^{1}H)$ chemical shifts between exchanging states, $^{1}H-^{15}N$ multiple-quantum dispersions are sensitive to changes in the chemical environments of *both* ^{1}H and ^{15}N spins. The resulting multiple-quantum relaxation dispersion profiles can, therefore, be quite different from those generated by single-quantum experiments, so that an analysis of both single- and multiple-quantum profiles together provides a powerful approach for obtaining robust measures of exchange parameters. This is particularly the case in applications to protonated proteins where other methods for studying exchange involving amide proton spins are negatively influenced by contributions from neighboring protons. The methodology is demonstrated on protonated and perdeuterated samples of a G48M mutant of the Fyn SH3 domain that exchanges between folded and unfolded states in solution.

Introduction

Insight into the relation between protein structure and function is often obtained from a study of static three-dimensional pictures that are generated from NMR or X-ray analyses of such molecules.[1] In many cases these structures provide important clues relating mechanism of action to molecular architecture. There are many other examples, however, of where such analyses fail. Biological molecules are not static and often undergo large-scale conformational rearrangements which are necessary for function.[2] The kinetics of such structural changes, the populations of the states that are involved in the rearrangements, and an atomic level description of the structures of intermediates along the reaction coordinate are all critical for understanding in detail the complex relation between structure and activity.

Characterization of states that may be only marginally populated is, however, difficult, since the majority of biophysical approaches are only sensitive to the most abundant species in solution.[3] In contrast, certain classes of relaxation-based NMR experiments can be exquisitely sensitive to the presence of minor conformers, so long as their populations exceed approximately 0.5% and the exchange kinetics lie in the microsecond−millisecond time regime.[4] In such cases, information on the kinetics and thermodynamics of the exchange process, as well as structural data on the minor states, can often be obtained. Examples in the literature include studies of millisecond (ms) time-scale dynamics as they relate to enzyme catalysis,[5−7] protein folding,[8,9] ligand binding,[10−13] and protein isomerization.[14,15]

In the past several years, a significant effort has been made to develop Carr−Purcell−Meiboom−Gill (CPMG)[16,17] NMR relaxation dispersion experiments that probe millisecond dynamics at both backbone and side chain positions in suitably

(1) Fersht, A. *Enzyme Structure and Mechanism*, 2nd ed.; Freeman & Co.: New York, 1985.
(2) Alber, T.; Gilbert, W. A.; Ponzi, D. R.; Petsko, G. A. *Ciba Found. Symp.* **1983**, *93*, 4−24.
(3) Fersht, A. *Structure and Mechanism in Protein Science*; W. H. Freeman and Company: New York, 1999.
(4) Palmer, A. G.; Kroenke, C. D.; Loria, J. P. *Methods Enzymol.* **2001**, *339*, 204−238.
(5) Eisenmesser, E. Z.; Bosco, D. A.; Akke, M.; Kern, D. *Science* **2002**, *295*, 1520−1523.
(6) Ishima, R.; Freedberg, D. I.; Wang, Y. X.; Louis, J. M.; Torchia, D. A. *Structure Fold Des.* **1999**, *7*, 1047−1055.
(7) Ishima, R.; Louis, J. M.; Torchia, D. A. *J. Mol. Biol.* **2001**, *305*, 515−21.
(8) Tollinger, M.; Skrynnikov, N. R.; Mulder, F. A. A.; Forman-Kay, J. D.; Kay, L. E. *J. Am. Chem. Soc.* **2001**, *123*, 11341−11352.
(9) Hill, R. B.; Bracken, C.; DeGrado, W. F.; Palmer, A. G. *J. Am. Chem. Soc.* **2000**, *122*, 11610−11619.
(10) Mulder, F. A. A.; Hon, B.; Muhandiram, D. R.; Dahlquist, F. W.; Kay, L. E. *Biochemistry* **2000**, *39*, 12614−12622.
(11) Mulder, F. A. A.; Mittermaier, A.; Hon, B.; Dahlquist, F. W.; Kay, L. E. *Nat. Struct. Biol.* **2001**, *8*, 932−935.
(12) Mulder, F. A. A.; Hon, B.; Mittermaier, A.; Dahlquist, F. W.; Kay, L. E. *J. Am. Chem. Soc.* **2002**, *124*, 1443−1451.
(13) Tolkatchev, D.; Xu, P.; Ni, F. *J. Am. Chem. Soc.* **2003**, *125*, 12432−12442.
(14) Korzhnev, D. M.; Karlsson, B. G.; Orekhov, V. Y.; Billeter, M. *Protein Sci.* **2003**, *12*, 56−65.
(15) Grey, M. J.; Wang, C. Y.; Palmer, A. G. *J. Am. Chem. Soc.* **2003**, *125*, 14324−14335.
(16) Carr, H. Y.; Purcell, E. M. *Phys. Rev.* **1954**, *4*, 630−638.
(17) Meiboom, S.; Gill, D. *Rev. Sci. Instrum.* **1958**, *29*, 688−691.

10.1021/ja049968b CCC: $27.50

labeled proteins.[8,18−21] Most experiments have focused on quantifying exchange contributions to the relaxation of backbone ^{15}N, ^{1}H, ^{13}C$^{\alpha}$, and side chain methyl ^{13}C *single-quantum* transitions, although recently methods for measuring dispersion profiles of backbone ^{1}H-^{15}N *double-* and *zero-quantum* transitions have also been reported.[22] A goal of our work is to develop additional experiments to study the backbone amide group, exploiting as many different coherences as possible, so that all of the experiments together provide more robust and reliable measures of exchange. Here we present ^{1}H−^{15}N backbone *multiple-quantum* dispersion experiments in which variable numbers of refocusing pulses are applied on either ^{1}H or ^{15}N spins. These new schemes complement the single-quantum and double-/zero-quantum experiments that have appeared previously. It is shown that the multiple-quantum versions have, in many cases, a very different functional dependence on applied radio frequency field, relative to other dispersion experiments, and that this difference can be exploited to improve the reliability of the extracted exchange parameters. Applications to both perdeuterated and protonated ^{15}N-labeled samples of the G48M mutant of the Fyn SH3 domain, which undergoes exchange between unfolded and folded states,[23] are presented, illustrating the utility of the new methodology. A description of the theoretical aspects of the new experiments is also included.

Materials and Methods

Sample Preparation: ^{15}N-labeled, perdeuterated, amide-protonated (^{15}N/^{2}H) and ^{15}N-labeled, protonated (^{15}N/^{1}H) samples of the G48M mutant of the Fyn SH3 domain were prepared as described previously,[23] except that the perdeuterated protein was expressed in D_2O media using ^{12}C,^{2}H-glucose as the carbon source. The ^{15}N/^{2}H (^{15}N/^{1}H) samples used were 0.8 (1.3) mM in protein, 50 mM sodium phosphate, 0.2 mM EDTA, 0.05% NaN_3, pH 7, 10% D_2O.

NMR Spectroscopy: Relaxation dispersion experiments involving the ^{15}N/^{2}H (^{15}N/^{1}H) samples of the G48M Fyn SH3 domain were carried out at 25 (30) °C on Varian *Inova* spectrometers at field strengths of 11.7, 14.1, and 18.8 T (only 14.1 and 18.8 T for ^{15}N MQ studies of the ^{15}N/^{1}H protein). ^{15}N SQ dispersions were recorded for ^{15}N/^{2}H and ^{15}N/^{1}H samples using the pulse sequence of Tollinger et al.,[8] building on the relaxation-compensation scheme of Loria et al.[18] ^{1}H single-quantum (SQ) dispersions were measured for ^{15}N/^{2}H-labeled proteins using the pulse sequence of Ishima et al.[21] ^{15}N MQ dispersions for ^{15}N/^{2}H and ^{15}N/^{1}H samples (i.e., MQ dispersions with variable numbers of ^{15}N 180° refocusing pulses) were measured using experiments a and b of Figure 1, respectively. ^{1}H MQ dispersions were recorded for the ^{15}N/^{2}H sample only (see text for discussion) using pulse scheme c of Figure 1. All relaxation dispersion experiments were carried out by recording a set of 2D spectra with variable spacing, 2δ, between refocusing pulses of a CPMG sequence applied during a constant time delay,[8] $T = 4n\delta$.

Data sets were processed using NMRPipe software[24] and subsequently analyzed using MUNIN,[25] as described previously. The peak intensities, I_1, in spectra recorded for different $\nu_{CPMG} = 1/(4\delta)$ frequencies were converted into $R_{2,eff}$ values according to $R_{2,eff} = -1/T\cdot\ln\{I_1(\nu_{CPMG})/I_0\}$, where I_0 is the peak intensity when the constant time CPMG element is removed. Uncertainties in $R_{2,eff}$ were obtained on the basis of repeat measurements for at least two separate ν_{CPMG} values (in cases where errors in $R_{2,eff}$ were less than 2%, errors of 2% were assumed). Constant time delays, T, of 20 (40) ms were used for MQ (SQ) dispersion measurements except that T values of 20, 30 ms were used for recording ^{1}H SQ dispersions at 14.1 T, 18.8 T on the ^{15}N/^{2}H sample, respectively. Each relaxation dispersion profile consists of 10 to 18 points measured with ν_{CPMG} varied between 50 and 1000 Hz in ^{15}N MQ/SQ experiments and between 50 Hz and 2.5 (2.0) kHz in ^{1}H MQ (SQ) experiments. The resulting measuring times were approximately the same for all experiments, between 18 and 24 h per dispersion.

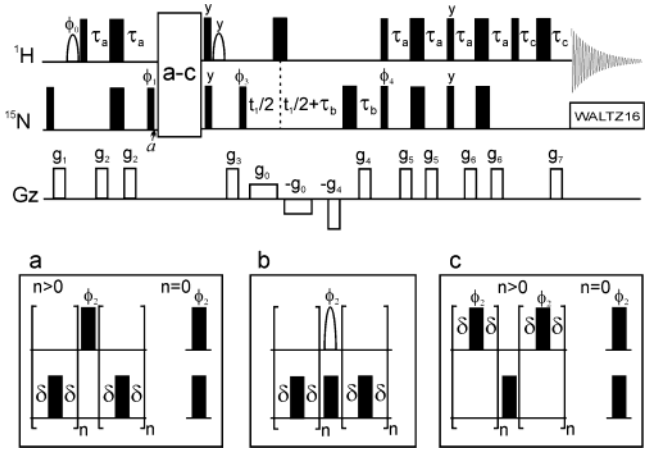

Figure 1. Pulse schemes for the measurement of ^{15}N (a and b) and ^{1}H MQ (c) dispersion profiles. Schemes a and c are used in applications involving perdeuterated proteins, while sequence b is designed for studies of protonated proteins (although it could also be used in applications to deuterated molecules). All narrow (wide) rectangular pulses are applied with a tip angle of 90° (180°) along the *x*-axis unless indicated otherwise. The shaped proton pulses (with the exception of the pulse of phase $\phi 2$ in scheme b) are water-selective and are typically implemented with "rectangular" shapes (∼ 2ms). All ^{15}N pulses are applied with a field of 5.8 kHz, with ^{15}N WALTZ-16 decoupling[35] achieved using a 1 kHz field (600 MHz). Schemes a and b: All rectangular ^{1}H pulses are applied with a 36 kHz field with the carrier centered on water, while the shaped 180° pulse of phase $\phi 2$ in scheme b has a RE-BURP profile[36] with an excitation maximum shifted to 8.1 ppm and a bandwidth that covers only the amide protons (at 600 MHz a 2.3 ms pulse is employed; the pulse is scaled according to 2.3*(600/*X*), where *X* is the spectrometer field). In scheme a the duration of the ^{1}H 180° pulse of phase $\phi 2$ is subtracted from the δ delays that immediately flank the pulse, while in scheme b an ^{15}N refocusing pulse is applied simultaneously with the RE-BURP pulse to refocus ^{15}N chemical shift evolution that would normally occur during the pulse. The water magnetization is preserved in both of these experiments. Scheme c: Water magnetization is dephased by moving the selective pulse of phase ϕ_0 prior to gradient g1 and eliminating the second water selective pulse (prior to g3). After the water-selective pulse, the ^{1}H carrier is jumped from water to the center of the amide region where it remains until prior to the ^{15}N 90° pulse of phase $\phi 3$, when it is returned to water. Non-selective ^{1}H pulses up to and including the 90_y pulse after the CPMG interval are applied with a field of 25 kHz, while the remaining pulses employ a 36 kHz field. One-half the duration of the ^{15}N 180° pulse applied in the center of the CPMG period is subtracted from each of the adjacent δ delays. The delays used are as follows: $\tau_a = 2.5$ ms, $\tau_b = 1.4$ ms, $\tau_c = 0.5$ ms. The phase cycling employed is as follows: $\phi_0 = \{-x\}$, scheme a; $\phi_0 = \{x\}$, scheme b; $\phi_1 = \{y,-y\}$; $\phi_2 = \{2(x),2(-x)\}$; $\phi_3 = \{4(x),4(-x)\}$; $\phi 4 = \{x\}$; rec = $\{2(x,-x),2(-x,x)\}$. Quadrature is achieved using the enhanced-sensitivity pulsed field gradient method[37,38] by incrementing phase $\phi 4$ by 180° and changing the sign of gradient g7. The durations and strengths of the gradients are as follows: $g_0 = (t_1/2, 0.5$ G/cm), $g_1 = (1$ ms, 6 G/cm), $g_2 = (0.5$ ms, 8 G/cm), $g_3 = (0.5$ ms, 14 G/cm), $g_4 = (1.25$ ms, 15 G/cm), $g_5 = (0.15$ ms, 15 G/cm), $g_6 = (0.15$ ms, 14 G/cm), $g_7 = (0.125$ ms, 29.5 G/cm).

Data Analysis: Measured relaxation dispersions for ^{15}N/^{2}H and ^{15}N/^{1}H G48M Fyn SH3 domain samples were analyzed on a per-residue

(18) Loria, J. P.; Rance, M.; Palmer, A. G. *J. Am. Chem. Soc.* **1999**, *121*, 2331−2332.
(19) Mulder, F. A. A.; Skrynnikov, N. R.; Hon, B.; Dahlquist, F. W.; Kay, L. E. *J. Am. Chem. Soc.* **2000**, *123*, 967−975.
(20) Skrynnikov, N. R.; Mulder, F. A. A.; Hon, B.; Dahlquist, F. W.; Kay, L. E. *J. Am. Chem. Soc.* **2001**, *123*, 4556−4566.
(21) Ishima, R.; Torchia, D. *J. Biomol. NMR* **2003**, *25*, 243−248.
(22) Orekhov, V., Yu; Korzhnev, D. M.; Kay, L. E. *J. Am. Chem. Soc.* **2004**, *126*, 1886−1891.
(23) Di Nardo, A. A.; Korzhnev, D. M.; Zarrine-Afsar, A.; Kay, L. E.; Davidson, A. R. *Proc. Natl. Acad. Sci.* **2004**, in press.
(24) Delaglio, F.; Grzesiek, S.; Vuister, G. W.; Zhu, G.; Pfeifer, J.; Bax, A. *J. Biomol. NMR* **1995**, *6*, 277−293.
(25) Korzhnev, D. M.; Ibraghimov, I. V.; Billeter, M.; Orekhov, V. Y. *J. Biomol. NMR* **2001**, *21*, 263−268.

basis. Namely, ^{1}H and ^{15}N MQ and SQ dispersion profiles for the ^{15}N/^{2}H-labeled protein recorded at three magnetic fields were fit numerically to a model of two-site exchange (states A and B). Values of the exchange rate constant, $k_{ex} = k_{AB} + k_{BA}$, and the population of the unfolded state, p_B, were treated as global adjustable parameters, while ^{1}H and ^{15}N chemical shift differences between states, $\Delta\varpi_H$ and $\Delta\varpi_N$, were adjusted separately for each type of dispersion. Thus, the 12 dispersion profiles recorded for each residue of the ^{15}N/^{2}H sample (^{1}H and ^{15}N MQ, SQ at three fields) were fit together using a total of 20 adjustable parameters: k_{ex}, p_B, $\Delta\varpi_H$ (^{1}H SQ), $\Delta\varpi_N$ (^{15}N SQ), $\Delta\varpi_H$ and $\Delta\varpi_N$ (^{1}H MQ), $\Delta\varpi_H$ and $\Delta\varpi_N$ (^{15}N MQ), and intrinsic relaxation rates at 11.7, 14.1, and 18.8 T for ^{1}H SQ, ^{15}N SQ, ^{1}H MQ, ^{15}N MQ coherences. Chemical shift differences extracted separately for each coherence have allowed us to address the consistency of the data recorded using SQ and MQ methods (see below). In what follows we will use $\Delta\varpi_i$ and $\Delta\omega_i$ to refer to chemical shift differences in ppm and rad/sec, respectively. *Moreover, all $\Delta\varpi_i$ values will be reported in ^{1}H ppm*, which will simplify the discussion that follows. ^{15}N MQ and SQ dispersion profiles for the ^{15}N/^{1}H sample were recorded at two and three magnetic fields, respectively, and analyzed together with k_{ex}, p_B, $\Delta\varpi_H$, and $\Delta\varpi_N$ as global parameters (so that a total of 5 dispersion profiles were fit using 9 adjustable parameters). This has allowed us to precisely estimate $\Delta\varpi_H$ without recording ^{1}H-based CPMG experiments that are only applicable for highly deuterated proteins. It should be noted that it is not possible to extract the sign of $\Delta\varpi_i$ from analyses of the dispersion profiles; only absolute values of $\Delta\varpi_i$ are reported in what follows. The quality of each fit was assessed using χ^2 statistics,[26] i.e. by comparison of the values of the χ^2 target function to the number of degrees of freedom in the optimized model. For all fits in Figures 3 and 4, reduced χ^2 values (χ^2/number of degrees of freedom) of less than 1 were obtained. Uncertainties in the extracted exchange parameters were estimated by the covariance matrix method.[27]

Experimental Artifacts: Simulations have established that MQ relaxation dispersion profiles are more sensitive to pulse offset effects than the corresponding SQ experiments. To evaluate the resulting systematic errors in $R_{2,eff}$, we have considered a two spin ^{15}N$-^1$H spin system, undergoing a two-site exchange process with exchange parameters similar to those determined for the ^{15}N/^{2}H-labeled G48M mutant of the Fyn SH3 domain, 25 °C (see below): $k_{ex} = 400$ s^{-1}, $p_B = 5\%$, $\Delta\varpi_N = 0.2, 0.4, 0.6$ ppm (^{1}H ppm) and $\Delta\varpi_H = 0, 0.1, 0.2, 0.3$ ppm. Simulations were performed in the space of 32 Cartesian operators, including the effects of relaxation for a system with an overall correlation time, τ_R, of 5 ns, $S^2 = 0.8$ and the time constant for fast internal motions, τ_e, set to 0. ^{15}N multiple-quantum CPMG dispersion profiles were generated with ν_{CPMG} ranging from 50 to 1000 Hz with a 50 Hz step size using a constant time relaxation period T of 40 ms along with an ^{15}N 180° pulse length of 80 μs and ^{15}N offsets from 0 to 10 ppm. All computations were done assuming a static B_o field of 18.8 T. The resulting dispersion profiles have been compared with those generated using an effective pulse width of 0 μs (i.e., zero pulse offset effects). A comparison of $R_{2,eff}$ values from the corresponding dispersions generated with and without offset effects establishes that the maximum difference is always less than 1.1 s^{-1} for ^{15}N offsets within 6 ppm (480 Hz). Simulations have also been performed to investigate the effect of differential relaxation between transverse elements (for example, H_XN_X) and the corresponding longitudinal terms that are present during application of the ^{15}N pulses (H_XN_Z in this case). Again a full density matrix treatment has been considered, taking into account, of course, relaxation. Exchange was not included in the computations so that flat dispersions are obtained in the absence of offset effects. For high ν_{CPMG} values ($> \sim$500 Hz), values of $R_{2,eff}$ increase as expected since $R(H_XN_X) = 0.5\{R(H_+N_+) + R(H_+N_-)\} < R(H_XN_Z)$. The extent of increase depends on offset and molecular size, so that, for $\tau_R = 5$ ns, calculated errors in $R_{2,eff}$ values are smaller than 1 s^{-1} for ^{15}N offsets less than 800 Hz, while, for $\tau_R = 15$ ns, the error can be as large as 1.5 s^{-1} for offsets of 800 Hz but less than 1 s^{-1} for offsets within 500 Hz. Interestingly, much of this error derives from a combination of offset and scalar coupling, since if the simulations are repeated with the one-bond ^{15}N$-^1$H coupling set to zero, the errors are reduced considerably. It is worth mentioning that a similar effect occurs for SQ dispersions, but in this case, dispersions decrease slightly with ν_{CPMG}, since $R(N_X) > R(N_Z)$.

We have also examined the effects of offset dependence on MQ dispersion profiles experimentally. A set of ^{15}N MQ dispersions were recorded on the ^{15}N/^{2}H G48M Fyn SH3 domain with the ^{15}N carrier placed at 114, 119, and 124 ppm. These profiles were supplemented with ^{15}N SQ dispersions recorded with the carrier at 119 ppm, since MQ data sets are best analyzed in concert with SQ profiles. For the 17 residues in the protein for which significant dispersions were obtained, each of the three ^{15}N MQ profiles was fit along with the ^{15}N SQ curve (data from both 14.1 and 18.8 T for a total of 4 curves/fit) to generate three sets of exchange parameters for a given residue (i.e., MQ data with the carrier at 114 ppm and SQ data were fit, MQ data with the carrier at 119 ppm and SQ data were fit, etc). Values of exchange parameters (k_{ex}, p_B, $\Delta\varpi_N$, $\Delta\varpi_H$) obtained for a given residue from any two fits are within error in cases where ^{15}N offsets are less than 6 ppm, consistent with the results from simulations. Notably, even when one of the exchange parameter sets is derived from fits involving ^{15}N MQ dispersions with offsets greater than 6 ppm (some as large as 15 ppm), in the majority of cases there is still good agreement (values are within experimental error) with parameters obtained from profiles that are more "on-resonance". Depending on the size of the dispersions and the errors that can be tolerated, it may be advisable to record ^{15}N MQ profiles at a pair of offsets, although this was not done in the present case. Note that for ^{1}H MQ dispersion measurements, offset effects are expected to be negligible due to the relatively short ^{1}H 180° pulses that are employed.

Results and Discussion

NMR Experiments. Figure 1 illustrates the new multiple-quantum CPMG-based dispersion experiments that have been developed to measure millisecond time-scale exchange processes in proteins. The schemes are similar to those reported previously for the generation of single-quantum (SQ) ^{15}N dispersion profiles,[8,18] and only the salient features will, therefore, be described here. At point *a* in the sequence, the coherence of interest is given by H_XN_X, where A_i, $i = \{x,y,z\}$ is the i component of A magnetization. In what follows below we will write $H_XN_X = (H_+N_+ + H_+N_- + H_-N_+ + H_-N_-)/4$, with $A_\pm = A_X \pm iA_Y$. The interval denoted by a$-$c in the figure is a constant time relaxation period during which CPMG trains of ^{15}N 180° pulses (a,b) or ^{1}H 180° pulses c are applied. Consider first schemes a and b. In both experiments multiple-quantum (MQ) dispersions are generated as a function of ^{15}N 180° pulse repetition rate (referred to in what follows as ^{15}N MQ dispersions). A single ^{1}H 180° pulse (phase $\phi 2$) is applied at the midpoint of the constant time interval ($T = 4n\delta$) which refocuses evolution from ^{1}H chemical shift. The experiments differ in that in scheme a the proton 180° pulse of phase $\phi 2$ is nonselective, while in scheme b an amide-proton selective pulse is employed. Thus, the latter scheme can be used in applications to protonated proteins, where evolution due to $^1H_{amide}-^1H_{aliphatic}$ scalar couplings is an issue, while for perdeuterated molecules either of sequences a or b can be employed (we have used scheme a here). In scheme b, an ^{15}N refocusing pulse is applied

(26) Zar, Z. H. *Biostatistical Analysis*; Prentice Hall Inc.: Englewood Cliffs, NJ, 1984.
(27) Press, W. H.; Flannery, B. P.; Teukolsky, S. A.; Vetterling, W. T. *Numerical Recipes in C*; Cambridge University Press: Cambridge, 1988.

simultaneously with the amide selective pulse to refocus ^{15}N chemical shift evolution during this interval (see legend to Figure 1). The additional ^{15}N pulse, relative to scheme a changes slightly the functional form of the resulting dispersions, provided they are recorded in a constant time manner (see below). After the constant time CPMG period, ^{15}N chemical shift is recorded and magnetization subsequently transferred back to ^{1}H for observation. A set of experiments is obtained with different values of δ and the effective relaxation rate, $R_{2,\mathrm{eff}}$, calculated for each site according to the relation $R_{2,\mathrm{eff}} = -1/T\cdot\ln\{I_1(\nu_{\mathrm{CPMG}})/I_0\}$, where $I_1(\nu_{\mathrm{CPMG}})$ (I_0) is the cross-peak intensity at the end of (in the absence of) the CPMG interval.

Sequence c generates ^{1}H MQ dispersion profiles and is similar to the ^{1}H SQ dispersion experiment, first described by Ishima and Torchia.[21] The ^{15}N pulse in the center of the CPMG element now assumes the role of the ^{1}H 180° ϕ2 pulse in (a) and in this case refocuses the ^{15}N chemical shift. As described by Ishima and Torchia,[21] application of schemes with variable numbers of ^{1}H pulses to protonated samples is complicated both by transverse cross-relaxation between amide and surrounding aliphatic spins and scalar coupled magnetization transfer, both of which vary with δ. Experiment c is, therefore, best performed on perdeuterated samples. The ^{1}H MQ scheme is likely to be less sensitive than the corresponding ^{15}N MQ sequences (a and b), since dephasing of water is necessary in the former case. Elimination of water magnetization avoids any ν_{CPMG} dependent signal intensity modulation that would otherwise occur due to increasing saturation of water with pulse number when nonselective ^{1}H pulses are used in the CPMG element (c). Note that water magnetization is preserved in the ^{15}N MQ experiments. Finally, it is worth pointing out that it is possible to develop a suite of multiple-quantum experiments in which variable numbers of ^{1}H refocusing pulses are inserted into the ^{15}N CPMG element (a,b) or ^{15}N pulses into the ^{1}H CPMG period (c) (rather than 1 used here), although we have not done so.

Theoretical Considerations: As described above, the MQ experiments of Figure 1 are similar to their SQ counterparts that have been discussed in the literature previously.[8,18,21] It might seem reasonable, therefore, to suppose that for a given set of exchange parameters the functional dependence of the dispersion profiles would be very similar for both SQ and MQ coherences. In fact, there can be some rather striking differences between the two classes of experiments, and it is worthwhile to develop the appropriate framework to appreciate some of these differences. In what follows we present a closed-form analytical expression for $R_{2,\mathrm{eff}}$ measured in MQ dispersion experiments as a function of δ. Such an equation is useful on a number of levels. First, by considering various limiting cases, insight can be obtained regarding how the various exchange parameters influence the resulting dispersions. Second, from a practical standpoint having an analytical expression expedites fitting of the dispersions; although data could be fit numerically (and we routinely do so) this is more computationally intensive. Third, such a derivation has been useful in clarifying the differences between measuring $R_{2,\mathrm{eff}}$ in constant time mode where only a single spectrum is recorded for each ν_{CPMG} value and from a series of time points (spectra) for each CPMG frequency.

Consider first a CPMG scheme of the form $(\delta\text{-}180_{\mathrm{N}}\text{-}\delta)_n\text{-}180_{\mathrm{H}}\text{-}(\delta\text{-}180_{\mathrm{N}}\text{-}\delta)_n$ with a constant time relaxation delay T ($T = 4n\delta$), and with the number of ^{15}N refocusing pulses variable (see Figure 1, sequence a; note that what follows also applies to sequence c, with "N" and "H" interchanged). We assume a system that undergoes two-site chemical exchange (sites A and B), with ^{1}H and ^{15}N frequency differences between the sites of $\Delta\omega_{\mathrm{H}}$ and $\Delta\omega_{\mathrm{N}}$, respectively, with equal relaxation rates, R, for zero- and double-quantum coherences in both states, and where the population of site A greatly exceeds that of B, $p_{\mathrm{A}} \gg p_{\mathrm{B}}$. Exchange is described by forward and reverse rate constants $k_{\mathrm{AB}} = k_{\mathrm{ex}}p_{\mathrm{B}}$, $k_{\mathrm{BA}} = k_{\mathrm{ex}}p_{\mathrm{A}}$. The effective relaxation rate for a given value of δ, $R_{2,\mathrm{eff}}$, is expressed as a function of signal attenuation as $-1/T\cdot\ln\{I_1/I_0\}$, where I_1 and I_0 are cross-peak intensities (state A) from experiments recorded with and without the CPMG period, respectively. At the start of the CPMG interval, the coherences of interest are given by the sum ($\mathbf{ZQ}_-$ + $\mathbf{ZQ}_+$ + $\mathbf{DQ}_-$ + $\mathbf{DQ}_+$)/4, with $\mathbf{DQ}_\pm = \{DQ_{\pm,\mathrm{A}}, DQ_{\pm,\mathrm{B}}\}^T$ and $\mathbf{ZQ}_\pm = \{ZQ_{\pm,\mathrm{A}}, ZQ_{\pm,\mathrm{B}}\}^T$ and double- (DQ) and zero- (ZQ) quantum states defined as the products of single-quantum ^{1}H and ^{15}N coherences, i.e., $ZQ_\pm = H_\mp N_\pm$ and $DQ_\pm = H_\pm N_\pm$. Therefore, the signal intensity at the end of the pulse sequence is calculated as the average over the components of magnetization originating from these four coherences.

The evolution of $\mathbf{DQ}_\pm$ and $\mathbf{ZQ}_\pm$ coherences during the free precession periods, δ, is given by $\mathbf{DQ}_\pm(\delta) = \mathbf{D}_\pm\mathbf{DQ}_\pm(0)$, $\mathbf{ZQ}_\pm(\delta) = \mathbf{Z}_\pm\mathbf{ZQ}_\pm(0)$ where

$$\mathbf{D}_\pm = \exp\left(\begin{bmatrix} -R - k_{\mathrm{ex}}p_{\mathrm{B}} & k_{\mathrm{ex}}p_{\mathrm{A}} \\ k_{\mathrm{ex}}p_{\mathrm{B}} & \pm i\Delta\omega_{\mathrm{H}} \pm i\Delta\omega_{\mathrm{N}} - R - k_{\mathrm{ex}}p_{\mathrm{A}} \end{bmatrix}\cdot\delta\right) \quad (1)$$

$$\mathbf{Z}_\pm = \exp\left(\begin{bmatrix} -R - k_{\mathrm{ex}}p_{\mathrm{B}} & k_{\mathrm{ex}}p_{\mathrm{A}} \\ k_{\mathrm{ex}}p_{\mathrm{B}} & \mp i\Delta\omega_{\mathrm{H}} \pm i\Delta\omega_{\mathrm{N}} - R - k_{\mathrm{ex}}p_{\mathrm{A}} \end{bmatrix}\cdot\delta\right)$$

Here we assume that the carrier frequencies of ^{1}H and ^{15}N pulses coincide with the resonance frequencies of magnetization in state A. The effect of ^{15}N 180° pulses is to interconvert $\mathbf{DQ}_\pm$ and $\mathbf{ZQ}_\mp$ coherences, while the single ^{1}H 180° pulse at the center of the interval T interconverts $\mathbf{DQ}_\pm$ and $\mathbf{ZQ}_\pm$ elements. Thus, $\mathbf{DQ}_\pm(4n\delta)$ and $\mathbf{ZQ}_\pm(4n\delta)$ that have evolved during the sequence $(\delta\text{-}180_{\mathrm{N}}\text{-}\delta)_n\text{-}180_{\mathrm{H}}\text{-}(\delta\text{-}180_{\mathrm{N}}\text{-}\delta)_n$ are given by

$$\mathbf{DQ}_\pm(4n\delta) = \mathbf{A}_\pm\mathbf{B}_\pm\mathbf{ZQ}_\pm(0) \quad (2)$$

$$\mathbf{ZQ}_\pm(4n\delta) = \mathbf{B}_\pm\mathbf{A}_\pm\mathbf{DQ}_\pm(0)$$

with $\mathbf{A}_\pm = (\mathbf{D}_\pm\mathbf{Z}_\mp\mathbf{Z}_\mp\mathbf{D}_\pm)^{n/2}$ and $\mathbf{B}_\pm = (\mathbf{Z}_\pm\mathbf{D}_\mp\mathbf{D}_\mp\mathbf{Z}_\pm)^{n/2}$. Implicit in eq 2 is the fact that $\mathbf{ZQ}_\pm(\mathbf{DQ}_\pm)$ coherences at the start of the CPMG delay evolve into $\mathbf{DQ}_\pm(\mathbf{ZQ}_\pm)$ by the end due to the action of the ^{1}H/^{15}N pulses during this interval. Note that $\mathbf{A}_+ = \mathbf{A}_-^*$, $\mathbf{B}_+ = \mathbf{B}_-^*$, $\mathbf{D}_+ = \mathbf{D}_-^*$, $\mathbf{Z}_+ = \mathbf{Z}_-^*$, $\mathbf{DQ}_+ = \mathbf{DQ}_-^*$, and $\mathbf{ZQ}_+ = \mathbf{ZQ}_-^*$, where * denotes complex conjugate. Therefore, expressions for $\mathbf{DQ}_-$ and $\mathbf{ZQ}_-$ coherences may be calculated simply by taking complex conjugates of those for $\mathbf{DQ}_+$ and $\mathbf{ZQ}_+$ (or simply by replacing $\Delta\omega_{\mathrm{H}}$ with $-\Delta\omega_{\mathrm{H}}$ and $\Delta\omega_{\mathrm{N}}$ with $-\Delta\omega_{\mathrm{N}}$).

The evolution matrices in eqs 1 and 2 are, in general, nonsymmetric. They can, however, always be symmetrized by the similarity transformation $\mathbf{X}' = \mathbf{S}^{-1}\mathbf{X}\mathbf{S}$, where $\mathbf{X}$ is one of $\mathbf{A}_\pm$, $\mathbf{B}_\pm$, $\mathbf{D}_\pm$, or $\mathbf{Z}_\pm$, $\mathbf{V}' = \mathbf{S}^{-1}\mathbf{V}$, $\mathbf{V}$ is equal to $\mathbf{DQ}_\pm$, $\mathbf{ZQ}_\pm$, and $\mathbf{S}$ is a diagonal matrix with elements, $S_{jk} = \sqrt{p_j}\delta_{jk}$.[28] Thus,

(28) Allerhand, A.; Thiele, E. *J. Chem. Phys.* **1966**, *45*, 902−916.

$\mathbf{DQ}_{\pm}(0)$, $\mathbf{ZQ}_{\pm}(0)$, assumed proportional to $\{p_A, p_B\}^T$, are transformed into $\mathbf{DQ'}_{\pm}(0)$, $\mathbf{ZQ'}_{\pm}(0)$ that are proportional to $\{\sqrt{p_A}, \sqrt{p_B}\}^T$. (Note that due to the preparation period proceeding the CPMG sequence initial conditions may deviate slightly from $\{p_A, p_B\}^T$). In the new notation eqs 1 and 2 are written as

$$\mathbf{D'}_{\pm} = \exp\left(\begin{bmatrix} -R - k_{ex}p_B & k_{ex}\sqrt{p_A p_B} \\ k_{ex}\sqrt{p_A p_B} & \pm i\Delta\omega_H \pm i\Delta\omega_N - R - k_{ex}p_A \end{bmatrix}\cdot\delta\right) \quad (3)$$

$$\mathbf{Z'}_{\pm} = \exp\left(\begin{bmatrix} -R - k_{ex}p_B & k_{ex}\sqrt{p_A p_B} \\ k_{ex}\sqrt{p_A p_B} & \mp i\Delta\omega_H \pm i\Delta\omega_N - R - k_{ex}p_A \end{bmatrix}\cdot\delta\right)$$

$$\mathbf{DQ'}_{\pm}(4n\delta) = \mathbf{A'}_{\pm}\mathbf{B'}_{\pm}\mathbf{ZQ'}_{\pm}(0)$$

$$\mathbf{ZQ'}_{\pm}(4n\delta) = \mathbf{B'}_{\pm}\mathbf{A'}_{\pm}\mathbf{DQ'}_{\pm}(0)$$

with $\mathbf{A'}_{\pm} = (\mathbf{D'}_{\pm}\mathbf{Z'}_{\mp}\mathbf{Z'}_{\mp}\mathbf{D'}_{\pm})^{n/2}$ and $\mathbf{B'}_{\pm} = (\mathbf{Z'}_{\pm}\mathbf{D'}_{\mp}\mathbf{D'}_{\mp}\mathbf{Z'}_{\pm})^{n/2}$. Symmetrization of the evolution matrices considerably simplifies the subsequent symbolic calculations.

The evolution of magnetization before and after the 180_H pulse is given by a weighted sum of two complex exponentials that correspond to the eigenvalues of $\mathbf{A'}_{\pm}$, $\mathbf{B'}_{\pm}$. It can be shown that $\mathbf{A'}_{+}$ and $\mathbf{B'}_{-}$ have the same eigenvalues and that the eigenvalues of $\mathbf{A'}_{-}$ and $\mathbf{B'}_{+}$ are complex conjugates of these. It can also be shown (at least numerically) that one of the two eigenvalues of $\mathbf{A'}_{+}$ and $\mathbf{B'}_{-}$ is equal to $\exp(-2n\delta\lambda_1)$, with λ_1 given by a modified Carver−Richards formula[29,30] that takes into account ^{1}H evolution during the ^{15}N CPMG period:

$$\lambda_1 = R + \frac{1}{2}\left(k_{ex} - \frac{1}{2\delta}\cosh^{-1}(D_+\cosh\eta_+ - D_-\cos\eta_-)\right) \quad (4)$$

where

$$D_{\pm} = \frac{1}{2}\left(\frac{\psi + 2\Delta\omega_N^2}{\sqrt{\psi^2 + \zeta^2}} \pm 1\right)$$

$$\eta_{\pm} = \sqrt{2}\delta\sqrt{\sqrt{\psi^2 + \zeta^2} \pm \psi}$$

$$\psi = (i\Delta\omega_H + (p_A - p_B)k_{ex})^2 - \Delta\omega_N^2 + 4p_A p_B k_{ex}^2$$

$$\zeta = -2\Delta\omega_N(i\Delta\omega_H + (p_A - p_B)k_{ex})$$

Note that λ_1 is a complex number with an imaginary part that approaches 0 in the limit $\Delta\omega_H \rightarrow 0$ and that in this limit eq 4 reduces to the original Carver−Richards formula for single-quantum coherence.[29,30] In most cases of interest, the decay of magnetization associated with the other eigenvalue, $\exp(-2n\delta\lambda_2)$, is too fast to be observed (i.e., $\mathrm{Re}(\lambda_2) \gg \mathrm{Re}(\lambda_1)$), and we have, therefore, neglected all such terms in the following derivation.

At the conclusion of the CPMG scheme $\mathbf{DQ'}_{+}(0) = {}^1/_4 M_0\{\sqrt{p_A}, \sqrt{p_B}\}^T$ has been converted into $\mathbf{ZQ'}_{+}(4n\delta)$ (see eq 2), and the "amount" of this coherence in state A is given by

$$I'_{1,D+} = {}^1/_4 M_0\left(\mathbf{B'}_{+}\mathbf{A'}_{+}\begin{bmatrix}\sqrt{p_A}\\ \sqrt{p_B}\end{bmatrix}\right)\cdot[1\ \ 0] = \quad (5)$$

$$= {}^1/_4 M_0\left((\mathbf{R}^T_{\mathbf{B'}+})\cdot\begin{bmatrix}\exp(-2n\delta\lambda_1^*) & 0\\ 0 & 0\end{bmatrix}\cdot(\mathbf{R}^T_{\mathbf{B'}+})^{-1}\cdot\right.$$

$$\left.(\mathbf{R}^T_{\mathbf{A'}+})\cdot\begin{bmatrix}\exp(-2n\delta\lambda_1) & 0\\ 0 & 0\end{bmatrix}\cdot(\mathbf{R}^T_{\mathbf{A'}+})^{-1}\cdot\begin{bmatrix}\sqrt{p_A}\\ \sqrt{p_B}\end{bmatrix}\right)\cdot[1\ \ 0]$$

and

$\mathbf{ZQ'}_{+}(0) = {}^1/_4 M_0\{\sqrt{p_A}, \sqrt{p_B}\}^T$
is converted into $\mathbf{DQ'}_{+}$ in the amount (state A):

$$I'_{1,Z+} = {}^1/_4 M_0\left(\mathbf{A'}_{+}\mathbf{B'}_{+}\begin{bmatrix}\sqrt{p_A}\\ \sqrt{p_B}\end{bmatrix}\right)\cdot[1\ \ 0] =$$

$${}^1/_4 M_0\left((\mathbf{R}^T_{\mathbf{A'}+})\cdot\begin{bmatrix}\exp(-2n\delta\lambda_1) & 0\\ 0 & 0\end{bmatrix}\cdot(\mathbf{R}^T_{\mathbf{A'}+})^{-1}\cdot\right.$$

$$\left.(\mathbf{R}^T_{\mathbf{B'}+})\cdot\begin{bmatrix}\exp(-2n\delta\lambda_1^*) & 0\\ 0 & 0\end{bmatrix}\cdot(\mathbf{R}^T_{\mathbf{B'}+})^{-1}\cdot\begin{bmatrix}\sqrt{p_A}\\ \sqrt{p_B}\end{bmatrix}\right)\cdot[1\ \ 0]$$

where $\mathbf{R}_{\mathbf{A'}+}$ and $\mathbf{R}_{\mathbf{B'}+}$ are matrices of eigenvectors of $\mathbf{A'}_{+}$ and $\mathbf{B'}_{+}$ (columns of $\mathbf{R}_{\mathbf{A'}+}$ and $\mathbf{R}_{\mathbf{B'}+}$ are the normalized eigenvectors of $\mathbf{A'}_{+}$, $\mathbf{B'}_{+}$) and $\mathbf{R}^T$ is the transpose of $\mathbf{R}$. Analogous expressions can be written for $I'_{1,D-}$ and $I'_{1,Z-}$, corresponding to the case where the coherences of interest at the start of the CPMG interval are $\mathbf{DQ'}_{-}$ and $\mathbf{ZQ'}_{-}$, respectively.

It remains to determine analytical expressions for $\mathbf{R}_{\mathbf{A'}+}$ and $\mathbf{R}_{\mathbf{B'}+}$. This can be accomplished by calculating expressions for $\mathbf{A'}_{\pm}$, $\mathbf{B'}_{\pm}$ (for $n = 2$) with the help of a symbolic calculation program such as Mathematica (Wolfram Research, Inc.) from which the matrices of eigenvectors can be obtained. It can be shown that $\mathbf{A'}_{\pm}$, $\mathbf{B'}_{\pm}$ are symmetric matrices with small off diagonal elements, and their matrices of eigenvectors are complex, antisymmetric:

$$\mathbf{R}^T_{\mathbf{A'}\pm} = \begin{bmatrix}1 - m_{D\pm}^2/2 & -m_{D\pm}\\ m_{D\pm} & 1 - m_{D\pm}^2/2\end{bmatrix},$$

$$\mathbf{R}^T_{\mathbf{B'}\pm} = \begin{bmatrix}1 - m_{Z\pm}^2/2 & -m_{Z\pm}\\ m_{Z\pm} & 1 - m_{Z\pm}^2/2\end{bmatrix} \quad (6)$$

$$(\mathbf{R}^T_{\mathbf{A'}\pm})^{-1} = \begin{bmatrix}1 - m_{D\pm}^2/2 & m_{D\pm}\\ -m_{D\pm} & 1 - m_{D\pm}^2/2\end{bmatrix},$$

$$(\mathbf{R}^T_{\mathbf{B'}\pm})^{-1} = \begin{bmatrix}1 - m_{Z\pm}^2/2 & m_{Z\pm}\\ -m_{Z\pm} & 1 - m_{Z\pm}^2/2\end{bmatrix}$$

where

$$m_{D\pm} = \pm\frac{ik_{ex}\sqrt{p_A p_B}}{d_{\pm}z_{\pm}}\left(z_{\pm} + 2\Delta\omega_N\frac{\sin(z_{\pm}\delta)}{\sin((d_{\pm} + z_{\pm})\delta)}\right) \quad (7)$$

$$m_{Z\mp} = \pm\frac{ik_{ex}\sqrt{p_A p_B}}{d_{\pm}z_{\pm}}\left(d_{\pm} - 2\Delta\omega_N\frac{\sin(d_{\pm}\delta)}{\sin((d_{\pm} + z_{\pm})\delta)}\right)$$

with $d_{\pm} = (\Delta\omega_H + \Delta\omega_N) \pm ik_{ex}$, $z_{\pm} = (\Delta\omega_H - \Delta\omega_N) \pm ik_{ex}$. Note that we have expanded the elements of the matrices of

(29) Carver, J. P.; Richards, R. E. *J. Magn. Reson.* **1972**, *6*, 89−105.
(30) Davis, D. G.; Perlman, M. E.; London, R. E. *J. Magn. Reson., Ser. B* **1994**, *104*, 266−275.

eigenvectors in a power series in $(p_A p_B)^{0.5}$, retaining terms up to and including $(p_A p_B)$.

Substituting eq 6 into eq 5, multiplying the matrices, and neglecting terms proportional to p_B^x with $x > 1$, or similarly, terms proportional to m_j^y with $y > 2$, $j = D_\pm, Z_\pm$, one can write $I'_{1,D\pm}$ and $I'_{1,Z\pm}$ as

$$I'_{1,D\pm} = {}^1/_4 M_0\sqrt{p_A}\exp(-2n\delta(\lambda_1 + \lambda_1^*))\cdot(1 - m_{D\pm}^2 + m_{D\pm}m_{Z\pm} - m_{Z\pm}^2 + m_{D\pm}\sqrt{p_B/p_A}) \quad (8)$$

$$I'_{1,Z\pm} = {}^1/_4 M_0\sqrt{p_A}\exp(-2n\delta(\lambda_1 + \lambda_1^*))\cdot(1 - m_{D\pm}^2 + m_{D\pm}m_{Z\pm} - m_{Z\pm}^2 + m_{Z\pm}\sqrt{p_B/p_A})$$

Recalling that $m_{D-} = m_{D+}^*$, $m_{Z-} = m_{Z+}^*$, that $I'_0 = M_0\sqrt{p_A}$ and that the net signal is proportional to the sum of the four coherences ($I'_{1,D\pm}$, $I'_{1,Z\pm}$) that are present at the end of the CPMG interval, the final expression for $R_{2,\mathrm{eff}}$ is calculated to be

$$R_{2,\mathrm{eff}}(1/(2\delta)) = \mathrm{Re}(\lambda_1) - \frac{1}{4n\delta}\ln\left(\mathrm{Re}\left(1 - m_{D+}^2 - m_{Z+}^2 + m_{D+}m_{Z+} + \frac{m_{D+} + m_{Z+}}{2}\sqrt{\frac{p_B}{p_A}}\right)\right) \quad (9)$$

with λ_1 given by eq 4 and m_{D+}, m_{Z+} by eq 7. Equation 9 is valid over the same range of exchange parameters for which the Carver−Richards equation[29,30] holds. Of interest, in the limit that $\delta \rightarrow 0$, the second term of eq 9 becomes $-1/(4n\delta)\ln(1 + 4\Delta\omega_H^2 k_{ex}^2 p_B/(\Delta\omega_H^2 + k_{ex}^2)^2)$.

Equation 9 is sufficiently compact that efficient back-calculations of model exchange parameters from experimental dispersion profiles can be performed using standard mathematical packages. Note that in principle $R_{2,\mathrm{eff}}$ may be written as a real function (i.e., real variables). However, for the sake of compactness, we prefer the functional form for $R_{2,\mathrm{eff}}$ given by eqs 4, 7, and 9.

It is worth emphasizing that the second term of eq 9, which provides a small correction to $\mathrm{Re}(\lambda_1)$ (see below), does not vanish in the limit that $\Delta\omega_H \rightarrow 0$, where multiple-quantum dispersions become identical to those measured in single-quantum experiments. Thus, the Carver−Richards equation (eq 4), which provides an estimate for $\mathrm{Re}(\lambda_1)$, *cannot rigorously be used as is* to analyze either SQ or MQ dispersion data generated when a constant time CPMG period is employed with $R_{2,\mathrm{eff}}$ given by $-1/T\cdot\ln\{I_1/I_0\}$, although the errors that do arise are very small for $T > 20-30$ ms in the case of SQ data and somewhat larger for MQ dispersions. (Note that the second term of eq 9 scales as $1/T$.) This can be understood clearly by recasting eq 9 as $I_1 = I_0 Q\exp(-4n\delta\mathrm{Re}(\lambda_1))$, with Q a function of δ but not n (or $T = 4n\delta$). For each δ value, the magnetization decay as a function of T is given by a single exponential with a rate of $\mathrm{Re}(\lambda_1)$, so that if dispersion experiments are recorded in a non-constant time manner by measuring several T points and obtaining the decay of signal as a function of T, $R_{2,\mathrm{eff}}$ is indeed given by $\mathrm{Re}(\lambda_1)$ (eq 4).

The analytical expression for $R_{2,\mathrm{eff}}$ for the CPMG-type scheme presented in Figure 1b, $(\delta\text{-}180_N\text{-}\delta)_n\text{-}180_{H,N}\text{-}(\delta\text{-}180_N\text{-}\delta)_n$, where $180_{H,N}$ indicates the simultaneous application of ^{1}H and ^{15}N 180° pulses in the center of the CPMG period, is slightly different than that presented in eq 9. For this particular scheme, evolution of the coherences $\mathbf{DQ'}_\pm$ and $\mathbf{ZQ'}_\pm$ is given by

$$\mathbf{DQ'}_\mp(4n\delta) = \mathbf{A'}_\mp\mathbf{A'}_\pm\mathbf{DQ'}_\pm(0) \quad (10)$$

$$\mathbf{ZQ'}_\mp(4n\delta) = \mathbf{B'}_\mp\mathbf{B'}_\pm\mathbf{ZQ'}_\pm(0)$$

where $\mathbf{A'}_\pm = (\mathbf{D'}_\pm\mathbf{Z'}_\mp\mathbf{Z'}_\mp\mathbf{D'}_\pm)^{n/2}$, $\mathbf{B'}_\pm = (\mathbf{Z'}_\pm\mathbf{D'}_\mp\mathbf{D'}_\mp\mathbf{Z'}_\pm)^{n/2}$, and $\mathbf{D'}_\pm$ and $\mathbf{Z'}_\pm$ are given by eq 3. In complete analogy to the derivation described above, one may write the expressions for $I'_{1,D\pm}$ and $I'_{1,Z\pm}$ in this case:

$$I'_{1,D\pm} = {}^1/_4 M_0\sqrt{p_A}\exp(-2n\delta(\lambda_1 + \lambda_1^*))\cdot(1 - m_{D\pm}^2 + m_{D\pm}m_{D\mp} - m_{D\mp}^2 + m_{D\pm}\sqrt{p_B/p_A}) \quad (11)$$

$$I'_{1,Z\pm} = {}^1/_4 M_0\sqrt{p_A}\exp(-2n\delta(\lambda_1 + \lambda_1^*))\cdot(1 - m_{Z\pm}^2 + m_{Z\pm}m_{Z\mp} - m_{Z\mp}^2 + m_{Z\pm}\sqrt{p_B/p_A})$$

Again, recalling that $m_{D-} = m_{D+}^*$, $m_{Z-} = m_{Z+}^*$, and $I'_0 = M_0\sqrt{p_A}$, $R_{2,\mathrm{eff}}$ measured using this constant time sequence is

$$R_{2,\mathrm{eff}}(1/(2\delta)) = \mathrm{Re}(\lambda_1) - \frac{1}{4n\delta}\ln\left(\mathrm{Re}\left(1 - m_{D+}^2 - m_{Z+}^2 + \frac{m_{D+}m_{D-} + m_{Z+}m_{Z-}}{2} + \frac{m_{D+} + m_{Z+}}{2}\sqrt{\frac{p_B}{p_A}}\right)\right) \quad (12)$$

We conclude this section with a few words about some of the assumptions that have been made in the above derivations. First, although eqs 9 and 12 are derived explicitly for the case where n is even, numerical simulations show that these expressions may be applied for any integral value of n. Second, we have assumed that the intrinsic relaxation rates are equivalent in both states, and indeed for many exchanging systems this will not be the case. For example, in the case of the exchanging SH3 domain considered below, relaxation rates in the unfolded and folded states differ by a factor of 2.[31] Palmer and co-workers have shown, however, that in the limit that $p_A \gg p_B$, dispersion profiles are rather insensitive to imbalances in relaxation rates.[32] Simulations that we have performed confirm this and establish that even for an unfolding system, contributions to dispersion profiles due to differences in relaxation rates are likely to be within noise (so long as $p_A \gg p_B$, as is the case for the G48M Fyn SH3 domain; see below). Third, we have assumed that double- and zero-quantum coherences relax with the same intrinsic rates, eq 1. This is not limiting; refocusing pulses applied during the course of the CPMG scheme interconvert DQ and ZQ states so that the effective intrinsic relaxation rate becomes $R(H_xN_x)$.

MQ Dispersion Profiles: Equations 1, 4, 9, and 12 above show a dependence on $\Delta\omega_H$ that is lacking in the case of exchange involving single-quantum ^{15}N magnetization, and this introduces a number of interesting features into the dispersion profiles, as illustrated in Figure 2. Figure 2a shows a series of ^{15}N MQ dispersion profiles generated for a two-site exchange process with $\Delta\varpi_N = \Delta\varpi_H = 0.25$ ppm (11.7 T), $p_A = 96\%$ and k_{ex} ranging from 250 to 2000 s^{-1}. (As described in Materials and Methods, $\Delta\omega_N$, $\Delta\omega_H$ are in units of rad/s, $\Delta\varpi_N$, $\Delta\varpi_H$ are

(31) Farrow, N. A.; Zhang, O.; Forman-Kay, J. D.; Kay, L. E. *Biochemistry* **1997**, *36*, 2390−2402.
(32) Millet, O.; Loria, J. P.; Kroenke, C. D.; Pons, M.; Palmer, A. G. *J. Am. Chem. Soc.* **2000**, *122*, 2867−2877.

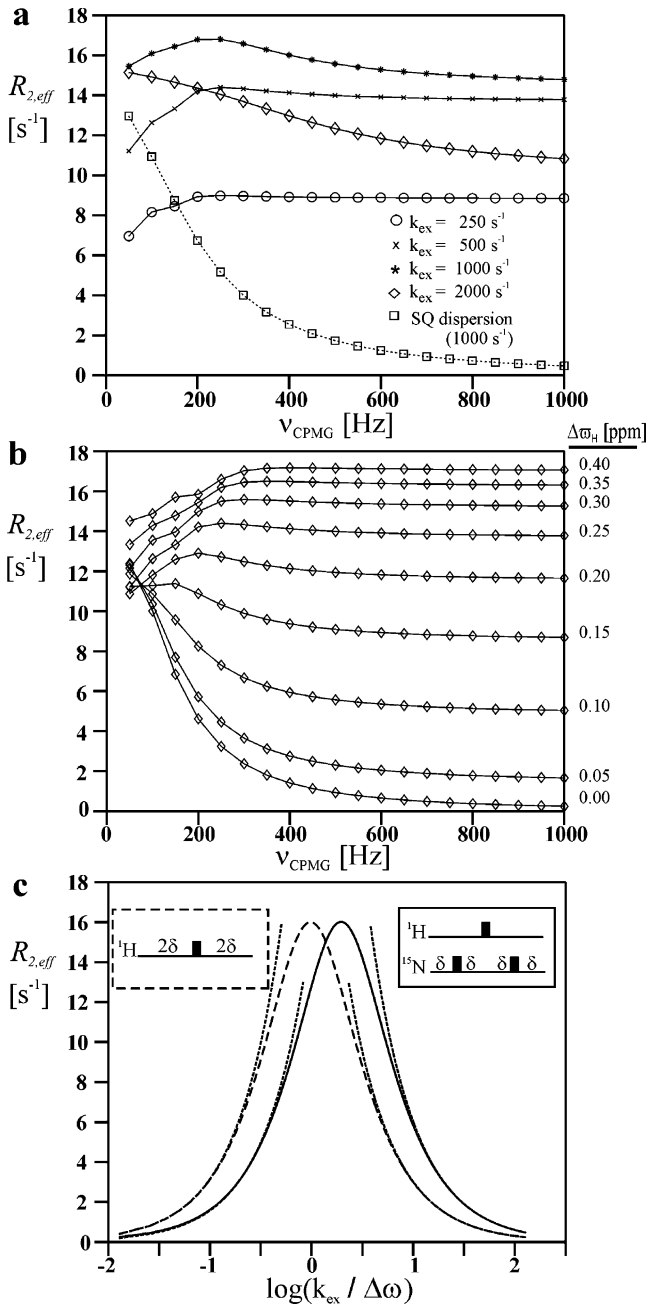

Figure 2. Simulated ^{15}N multiple-quantum dispersion profiles illustrating the effect of nonzero values of $\Delta\omega_H$ on the dispersions. (a) Dispersion profiles generated from scheme a of Figure 1, $T = 4n\delta = 40$ ms, and computed for a two-site exchange process (eqs 1 and 2) with $\Delta\varpi_N = \Delta\varpi_H = 0.25$ ppm (11.7 T field; *all ppm values listed here and below are ^{1}H ppm*), $p_A = 96\%$, are illustrated as a function of k_{ex}. A reference ^{15}N single-quantum dispersion profile is shown with $k_{ex} = 1000$ s^{-1} (otherwise the same parameters as above). (b) Dispersion profiles ($\Delta\varpi_N = 0.25$ ppm, 11.7 T field, $p_A = 96\%$, $k_{ex} = 500$ s^{-1}) as a function of $\Delta\varpi_H$, ranging from 0 to 0.4 ppm (indicated on the right-hand side of the figure). (c) Simulated $R_{2,eff}(\nu_{CPMG} \rightarrow 0)$ (solid curve) and $R_{2,eff}(\nu_{CPMG} \rightarrow \infty)$ (dashed curve) as a function of $\log(k_{ex}/\Delta\omega)$ for $\Delta\varpi_N = \Delta\varpi_H = 0.25$ ppm (11.7 T field), $p_A = 96\%$ ($\Delta\omega = \Delta\omega_N = \Delta\omega_H = 250\pi$). As discussed in the text, the slow ($R_{2,eff}(\nu_{CPMG} \rightarrow 0)$) and fast ($R_{2,eff}(\nu_{CPMG} \rightarrow \infty)$) pulsing limits can be approximated using the sequences on the right (^{1}H$-^{15}$N multiple-quantum coherence, $\delta \rightarrow \infty$) and left (^{1}H single-quantum coherence), respectively. Also plotted (dotted lines) are k_{AB}, $k_{AB}/2$ (slow exchange limit, left) and $p_A p_B(\Delta\omega)^2/k_{ex}$, $^1/_2 p_A p_B(2\Delta\omega)^2/k_{ex}$ (fast exchange limit, right). See text for details.

the equivalent, *both* expressed in ^{1}H ppm.) Profiles have been simulated numerically (identical dispersions are generated using eq 9) assuming the pulse scheme of Figure 1a with $T = 4n\delta = 40$ ms. Very similar dispersions would be obtained if the sequence of Figure 1b were employed. The ^{15}N single-quantum dispersion profile is shown (open squares) as a point of reference ($k_{ex} = 1000$ s^{-1}). For large k_{ex} values, $R_{2,eff}$ profiles look not unlike those for single-quantum magnetization in the sense that $R_{2,eff}$ values decrease with increasing ν_{CPMG} (for example, $k_{ex} = 2000$ s^{-1}). However, as illustrated in the figure, as k_{ex} decreases from 2000 s^{-1}, the dispersions become more shallow, and when $k_{ex} = 500$, 250 s^{-1}, profiles that increase as a function of ν_{CPMG} (at least for low values of ν_{CPMG}) are obtained!

Figure 2b illustrates the influence of $\Delta\omega_H$ on ^{15}N MQ dispersion profiles for two-site exchange with parameters $\Delta\varpi_N = 0.25$ ppm (11.7 T), $p_A = 96\%$, and $k_{ex} = 500$ s^{-1}. In the case where $\Delta\varpi_H = 0$ ppm, multiple-quantum and single-quantum dispersions are equivalent and an $R_{2,eff}$ profile that decreases significantly with ν_{CPMG} is obtained. As $\Delta\varpi_H$ increases, however, the dispersions become smaller, gradually becoming concave in shape. The origin of this surprising transition can be understood by considering the difference in $R_{2,eff}$ rates for very small and very large ν_{CPMG} values (R_{ex}) in a number of limiting cases. Note that for large ν_{CPMG} values, exchange contributions arising from $\Delta\omega_N$ are effectively quenched and $R_{2,eff}$ rates for ^{1}H$-^{15}$N multiple-quantum coherences can be derived by considering the evolution of single-quantum ^{1}H magnetization during the element illustrated in the dashed box in Figure 2c (contributions to $R_{2,eff}$ of k_{AB} and $p_A p_B(\Delta\omega_H)^2/k_{ex}$ in the slow and fast exchange limits, respectively[4]). In contrast, for $\nu_{CPMG} \approx 0$, $R_{2,eff}$ rates are calculated from the inset on the right side of Figure 2c with $\delta \rightarrow \infty$. Consider an exchanging system with $\Delta\omega_N = \Delta\omega_H = \Delta\omega$ so that only the double-quantum component is relaxed due to exchange (eq 1). In the slow pulsing limit, exchange is operative only 50% of the time, since double- and zero-quantum coherences are interconverted and allowed to evolve for intervals of equal duration and exchange influences only double-quantum coherences. From the above discussion, the value of $R_{2,eff}(\nu_{CPMG} \rightarrow 0)$ and $R_{2,eff}(\nu_{CPMG} \rightarrow \infty)$ can be calculated from the schemes on the right (with $\delta \rightarrow \infty$) and left, respectively. Assuming fast exchange, $R_{2,eff}(\nu_{CPMG} \rightarrow 0) = {}^1/_2 p_A p_B(2\Delta\omega)^2/k_{ex}$ and $R_{2,eff}(\nu_{CPMG} \rightarrow \infty) = p_A p_B(\Delta\omega)^2/k_{ex}$ (contributions to $R_{2,eff}$ from intrinsic relaxation are neglected), and thus, a dispersion profile is obtained which decreases with ν_{CPMG} (Figure 2a, diamond symbols for example). In the case of slow exchange, $R_{2,eff}(\nu_{CPMG} \rightarrow 0) = k_{AB}/2$, since only the double-quantum component is affected by exchange, while $R_{2,eff}(\nu_{CPMG} \rightarrow \infty) = k_{AB}$ and a dispersion profile is obtained that increases with increasing ν_{CPMG} (Figure 2a, open circles, for example).

In Figure 2c, contributions to $R_{2,eff}$ in the slow ($4\delta = 1$ s, solid curve) and fast pulsing (dashed curve) limits as a function of $k_{ex}/\Delta\omega$ are shown for $\Delta\varpi_N = \Delta\varpi_H = 0.25$ ppm (11.7 T) and $p_A = 96\%$. Dispersions with $R_{2,eff}(\nu_{CPMG} \rightarrow 0) < R_{2,eff}(\nu_{CPMG} \rightarrow \infty)$ are those derived from $k_{ex}/\Delta\omega$ ratios for which the dashed curve is higher than the solid curve in the figure. Also shown in the figure are the curves corresponding to $R_{2,eff} = k_{AB}/2$ and k_{AB} (slow exchange limit, slow and fast pulsing, respectively, dotted lines on the left) and $^1/_2 p_A p_B(2\Delta\omega)^2/k_{ex}$, $p_A p_B(\Delta\omega)^2/k_{ex}$ (fast exchange limit, slow and fast pulsing, respectively, dotted lines on the right). Of interest, good agreement between the exact contributions (solid/dashed curves)

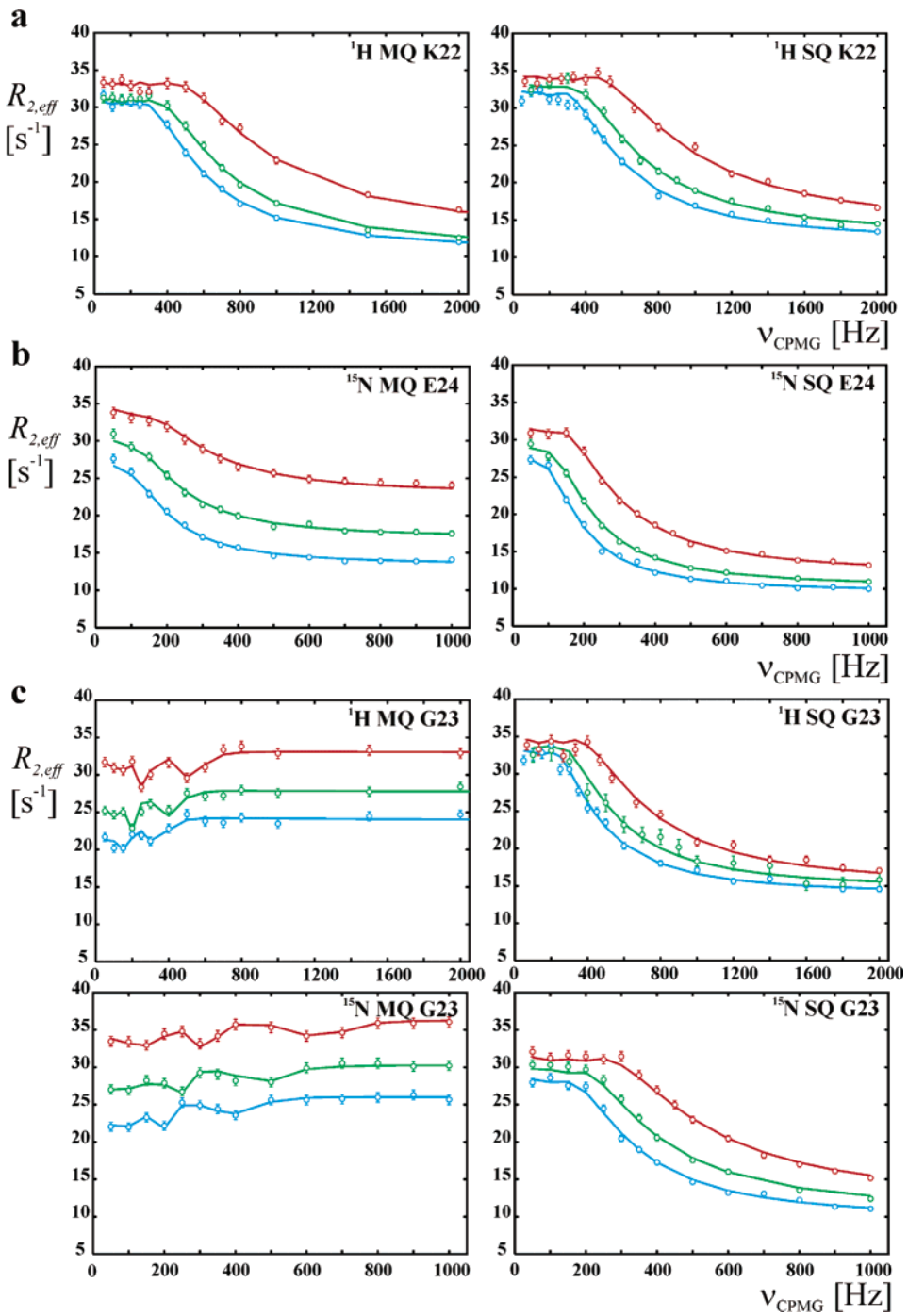

Figure 3. Selected ^{1}H, ^{15}N MQ and SQ dispersion profiles for K22 (a), E24 (b), and G23 (c) recorded on a perdeuterated, ^{15}N-labeled sample of the G48M Fyn SH3 domain, 25 °C. Dispersions recorded at 11.7, 14.1, and 18.8 T are color-coded blue, green, and red, respectively. Experimental data points are indicated by circles, with best fit curves generated from global fits of all dispersion data from a single residue shown with solid lines. In part c, 6 s^{-1} and 3 s^{-1} has been subtracted from ^{1}H,^{15}N MQ curves recorded at 11.7 and 14.1 T, respectively, to aid in presentation. ^{15}N dispersions for K22 as well as ^{1}H dispersions for E24 are relatively flat and are therefore not displayed. See text for details.

and contributions calculated in the slow and fast exchange limits (dotted curves) are obtained over a wide range of $k_{ex}/\Delta\omega$ values.

Implicit in eqs 9 and 12 above (and established with experimental data below) is that both $\Delta\varpi_H$ and $\Delta\varpi_N$ can be extracted from a given ^{1}H or ^{15}N MQ dispersion profile. The MQ experiments are thus particularly powerful in that two chemical shift differences can be obtained. A second important point concerns the functional form of the dispersion profiles. As illustrated in Figure 2 and below in Figures 3 and 4, SQ and MQ dispersion profiles can be quite different and this difference contributes to robustness in the extraction of exchange parameters. Note that the dispersions generated in Figure 2 were obtained using $\Delta\varpi_N = \Delta\varpi_H = 0.25$ ppm (^{1}H ppm). For a system exchanging between folded and unfolded states, it is often the case that larger $\Delta\omega$ values are obtained. In these cases and when $\Delta\varpi_N \approx \Delta\varpi_H$, the resulting ^{15}N MQ dispersion profiles do not increase monotonically with ν_{CPMG}, as in Figure 2, but rather exhibit oscillations at low ν_{CPMG} that may be useful in some cases for improving the precision of the extracted exchange parameters (see Figure 3, below).

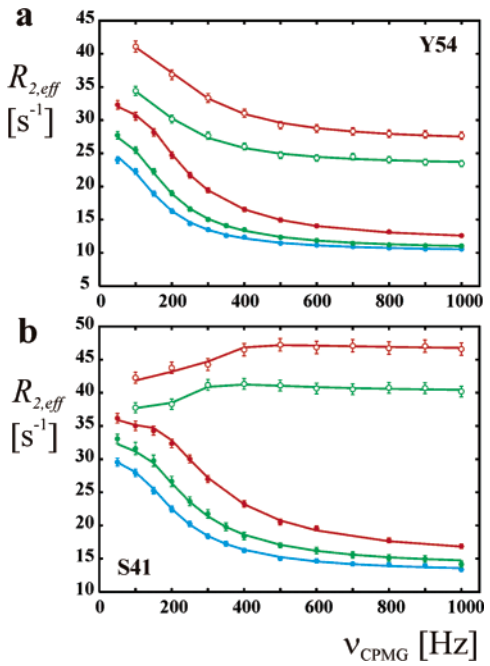

Figure 4. ^{15}N MQ (upper two traces) and ^{15}N SQ dispersion profiles (bottom three) recorded for Y54 (a) and S41 (b) of a protonated ^{15}N sample of the G48M Fyn SH3 domain, 30 °C (red, green, and blue color-coded for 18.8, 14.1, and 11.7 T). Experimental MQ(SQ) data points are indicated with open(filled) circles, with curves generated from global fits of the data shown with solid lines (see text for details).

Applications to the G48M Fyn SH3 Domain: The pulse schemes described above have been applied to an SH3 domain from the Fyn tyrosine kinase that has been shown by a variety of techniques including fluorescence spectroscopy and ^{15}N SQ relaxation dispersion NMR methodology to exchange between folded and unfolded states.[23] Figure 3 shows ^{1}H and ^{15}N MQ dispersion profiles for a number of residues from the ^{15}N/^{2}H-labeled Fyn SH3 domain sample, along with the corresponding ^{1}H and ^{15}N SQ profiles for comparison, 25 °C. We have chosen to present SQ and MQ dispersions to illustrate some of the unique features of the MQ data. In a subsequent publication, a comprehensive analysis of SQ, MQ and zero-/double-quantum data sets will be described. ^{1}H and ^{15}N MQ and SQ profiles (at 11.7 T-blue, 14.1 T-green, and 18.8 T-red) for each residue have been fit together (a total of 12 dispersion curves) to extract global exchange parameters, k_{ex}, p_B along with $\Delta\varpi_H$ (^{1}H SQ), $\Delta\varpi_N$ (^{15}N SQ), $\Delta\varpi_H$ and $\Delta\varpi_N$ (^{1}H MQ), $\Delta\varpi_H$ and $\Delta\varpi_N$ (^{15}N MQ), and intrinsic relaxation rates. We have chosen to extract chemical shift values separately from each curve so as to assess the consistency of the extracted parameters from one experiment to the next. All told, 20 adjustable parameters were used in fits of the 12 dispersion profiles.

Figure 3a shows fits (solid curves) of dispersion data (open circles) for K22, for which $\Delta\varpi_H \neq 0$, $\Delta\varpi_N \approx 0$. As is readily apparent from the figure, nearly identical ^{1}H MQ and SQ dispersion profiles are obtained (a consequence of $\Delta\varpi_N \approx 0$). Values of $k_{ex} = 430 \pm 80$ s^{-1}, $p_B = 4.7 \pm 0.8\%$, and $\Delta\varpi_H = 1.132 \pm 0.015$ ppm (chemical shift difference extracted from ^{1}H SQ dispersion data), $\Delta\varpi_N = 0.030 \pm 0.003$ ppm (^{15}N SQ, data not shown), $\Delta\varpi_H = 1.146 \pm 0.017$ ppm (^{1}H MQ), $\Delta\varpi_N = 0 \pm 7$ ppm (^{1}H MQ) are obtained (here and in what follows all shift differences are given in ^{1}H ppm). In Figure 3b, ^{15}N MQ and SQ profiles are shown for E24. Values of $k_{ex} = 370 \pm 20$ s^{-1}, $p_B = 5.6 \pm 0.2\%$, $\Delta\varpi_H = 0.089 \pm 0.002$ ppm (^{1}H SQ, data not shown), $\Delta\varpi_N = 0.345 \pm 0.005$ ppm (^{15}N SQ), $\Delta\varpi_H = 0.076 \pm 0.003$ ppm (^{15}N MQ), $\Delta\varpi_N = 0.348 \pm 0.007$ ppm (^{15}N MQ) are obtained. Of note, ^{15}N MQ profiles are smaller than the corresponding ^{15}N SQ curves for this residue, due to the finite $\Delta\varpi_H$; ^{15}N MQ dispersions decrease with increasing ν_{CPMG}, since $\Delta\varpi_H \ll \Delta\varpi_N$. Finally, in Figure 3c, ^{1}H, ^{15}N MQ and SQ profiles are illustrated for G23, a case where $\Delta\varpi_H \approx \Delta\varpi_N \neq 0$. It is interesting to note that in cases with large $\Delta\varpi$ values and where $\Delta\varpi_H \approx \Delta\varpi_N$, MQ dispersion profiles oscillate for low ν_{CPMG} values and do not decrease with increasing ν_{CPMG} frequencies. Quite remarkably, the (small) oscillations observed in the experimental data at low ν_{CPMG} values can be completely explained by theory. Exchange parameters $k_{ex} = 410 \pm 30$s^{-1}, $p_B = 4.9 \pm 0.3\%$ and shift differences $\Delta\varpi_H = 0.866 \pm 0.013$ ppm (^{1}H SQ), $\Delta\varpi_N = 0.626 \pm 0.008$ ppm (^{15}N SQ), $\Delta\varpi_H = 0.857 \pm 0.013$ ppm (^{1}H MQ), $\Delta\varpi_N = 0.646 \pm 0.008$ ppm (^{1}H MQ), $\Delta\varpi_H = 0.808 \pm 0.009$ ppm (^{15}N MQ), $\Delta\varpi_N = 0.637 \pm 0.014$ ppm (^{15}N MQ) are obtained. The extracted values of k_{ex} and p_B for each of the three residues shown in Figure 3 are in quite good agreement, as are residue- and coherence-specific $\Delta\varpi_i$ values obtained from the different profiles (compare for example $\Delta\varpi_H$ for G23 obtained from fits of ^{1}H SQ, ^{1}H MQ, and ^{15}N MQ dispersions).

Figure 4 shows ^{15}N MQ (open circles) and SQ (filled circles) dispersion profiles for Y54 and S41 measured at 30 °C on a protonated (^{15}N/^{1}H) G48M Fyn SH3 domain sample. As described above, it is difficult to record accurate ^{1}H dispersions on protonated samples,[21] and reliable $\Delta\varpi_H$ values are therefore not easily obtained from fits of data from such experiments. In contrast, values of $\Delta\varpi_H$ can be extracted from fits of ^{15}N MQ dispersion profiles. The sensitivity of such profiles to $\Delta\varpi_H$ is quite apparent from a comparison of SQ and MQ dispersions of Y54 and S41, Figure 4, where it is clear that $\Delta\varpi_H$ is much smaller for Y54 than for S41. ^{15}N MQ and SQ dispersion profiles from the protonated sample were fit together with k_{ex}, p_B, $\Delta\varpi_H$, and $\Delta\varpi_N$ treated as global parameters, allowing extraction of accurate values for $\Delta\varpi_H$. Exchange parameters of $k_{ex} = 640 \pm 14$ s^{-1}, $p_B = 4.2 \pm 0.1\%$, $\Delta\varpi_H = 0.051 \pm 0.002$ ppm, $\Delta\varpi_N = 0.259 \pm 0.002$ ppm for Y54 and $k_{ex} = 672 \pm 24$s^{-1}, $p_B = 3.6 \pm 0.1\%$, $\Delta\varpi_H = 0.285 \pm 0.006$ ppm, $\Delta\varpi_N = 0.361 \pm 0.004$ ppm for S41 (all ^{1}H ppm) were obtained. It is interesting to compare these extracted values with those measured for the same residues in the deuterated sample, with the caveat that experiments on the protonated sample were recorded at a temperature 5 °C higher than on the deuterated protein. For Y54 in the perdeuterated sample, we measure $k_{ex} = 365 \pm 20$ s^{-1}, $p_B = 6.0 \pm 0.2\%$, $\Delta\varpi_H$(avg) $= 0.086 \pm 0.040$ ppm and $\Delta\varpi_N$(avg) $= 0.284 \pm 0.012$ ppm, where $\Delta\varpi_i$(avg) is the average over the three values obtained from fits of the SQ and MQ dispersions, with the standard deviation reported as well. In the case of S41, $k_{ex} = 360 \pm 34$ s^{-1}, $p_B = 4.7 \pm 0.4\%$, $\Delta\varpi_H$(avg) $= 0.291 \pm 0.036$ ppm, $\Delta\varpi_N$(avg) $= 0.364 \pm 0.006$ ppm. The chemical shift differences are in excellent agreement between protonated and deuterated samples, with p_B values considerably higher in the case of the deuterated sample, indicating that perdeuteration decreases the stablity of the G48M Fyn SH3 domain. The above data is also consistent with a decrease in the folding rate upon deuteration, with a small change to the unfolding rate, again reflecting loss of stability.

The effect of deuteration on protein stability has been documented,[33,34] and in some cases stability decreases of the sort observed here have been noted.[33]

In summary, we have presented pulse schemes for the measurement of ^{15}N and ^{1}H MQ dispersion profiles. These new sequences are powerful additions to the repertoire of experiments that are available for studying exchanging systems. MQ and SQ dispersion curves can be fit simultaneously to obtain more robust measures of exchange parameters than would be possible from independent fits. This is particularly the case when one considers that the dependence of MQ and SQ profiles on ν_{CPMG} can be quite different. In the case of protonated samples, recording ^{15}N MQ profiles allows extraction of $\Delta\varpi_H$ values that would be difficult to obtain using other types of dispersion experiments. The theory behind the experiments has been presented, along with analytical expressions that permit rapid extraction of exchange parameters from fits of the data. Finally, the utility of the experiments has been established with applications to protonated and perdeuterated samples of an SH3 domain that exchanges between folded and unfolded states.

(33) Hattori, A.; Crespi, H. L.; Katz, J. J. *Biochemistry* **1965**, *12*, 13−25.
(34) Rokop, S.; Gajda, L.; Parmerter, S.; Crespi, H. L.; Katz, J. J. *Biochim. Biophys. Acta* **1969**, *191*, 707−715.
(35) Shaka, A. J.; Keeler, J.; Frenkiel, T.; Freeman, R. *J. Magn. Reson.* **1983**, *52*, 335−338.
(36) Geen, H.; Freeman, R. *J. Magn. Reson.* **1991**, *93*, 93−141.
(37) Kay, L. E.; Keifer, P.; Saarinen, T. *J. Am. Chem. Soc.* **1992**, *114*, 10663−10665.
(38) Schleucher, J.; Sattler, M.; Griesinger, C. *Angew. Chem., Int. Ed. Engl.* **1993**, *32*, 1489−1491.

Acknowledgment. This work was supported by a grant from the Canadian Institutes of Health Research (C.I.H.R.) to L.E.K. The authors are grateful to Prof. Alan Davidson and Dr. Ariel A. DiNardo for kindly providing samples used in this study. Thanks are extended to Prof. Nikolai Skrynnikov (Purdue University) and Dr. Vladislav Orekhov (Swedish NMR Center, Goteborg) for valuable discussions at the start of the project. D.M.K. is the recipient of a C.I.H.R. Training Grant Postdoctoral Fellowship. L.E.K. holds a Canada Research Chair in Biochemistry.

JA049968B